Global and Planetary Change 129 (2015) 23–36

Contents lists available at ScienceDirect

Global and Planetary Change

journal homepage: www.elsevier.com/locate/gloplacha

Detecting changes in the transport of the Gulf Stream and the Atlantic overturning circulation from coastal sea level data: The extreme decline in 2009–2010 and estimated variations for 1935–2012

Tal Ezer *

Center for Coastal Physical Oceanography, Old Dominion University, 4111 Monarch Way, Norfolk, VA 23508, USA

ARTICLE INFO

Article history:
Received 21 January 2015
Received in revised form 3 March 2015
Accepted 9 March 2015
Available online 13 March 2015

Keywords:
Atlantic Meridional Overturning Circulation
Gulf Stream
sea level
climate change

ABSTRACT

Recent studies reported weakening in the Atlantic Meridional Overturning Circulation (AMOC) and in the Gulf Stream (GS), using records of about a decade (RAPID project) or two (altimeter data). Coastal sea level records are much longer, so the possibility of detecting climatic changes in ocean circulation from sea level data is intriguing and thus been examined here. First, it is shown that variations in the AMOC transport from the RAPID project since 2004 are consistent with the flow between Bermuda and the U. S. coast derived from the Oleander measurements and from sea level difference (SLDIF). Despite apparent disagreement between recent studies on the ability of data to detect weakening in the GS flow, estimated transport changes from 3 different independent data sources agree quite well with each other on the extreme decline in transport in 2009–2010. Due to eddies and meandering, the flow representing the GS part of the Oleander line is not correlated with AMOC or with the Florida Current, only the flow across the entire Oleander line from the U.S. coast to Bermuda is correlated with climatic transport changes. Second, Empirical Mode Decomposition (EMD) analysis shows that SLDIF can detect (with lag) the portion of the variations in the AMOC transport that are associated with the Florida Current and the wind-driven Ekman transport (SLDIF-transport correlations of ~0.7–0.9). The SLDIF has thus been used to estimate variations in transport since 1935 and compared with AMOC obtained from reanalysis data. The significant weakening in AMOC after ~2000 (~4.5 Sv per decade) is comparable to weakening seen in the 1960s to early 1970s. Both periods of weakening AMOC, in the 1960s and 2000s, are characterized by faster than normal sea level rise along the northeastern U.S. coast, so monitoring changes in AMOC has practical implications for coastal protection.

1. Introduction

Recent findings of acceleration in sea level rise (SLR) along the U.S. East Coast north of the separation point of the GS at Cape Hatteras, North Carolina (Boon, 2012; Ezer and Corlett, 2012; Sallenger et al., 2012; Ezer, 2013; Ezer et al., 2013; Kopp, 2013), suggest that this acceleration may be a dynamic response to changes in ocean circulation. (See Appendix A for definitions of all the acronyms used.) The stretch of the North American coast between Cape Hatteras and Cape Cod has been labeled a "hotspot for accelerated sea level rise" (Sallenger et al., 2012) and a "hotspot for accelerated flooding" (Ezer and Atkinson, 2014), thus it is important to study the implications of regional climatic changes for flood-prone coastal communities (Atkinson et al., 2013; Nicholls and Cazenave, 2010; Cazenave and Cozannet, 2014; Goddard et al., 2015) and better understand the forcing mechanism behind those changes. Note that part of the hotspot region, especially the lower Chesapeake Bay area, has additional contribution to the relative SLR from land subsidence associated with the Glacial Isostatic Adjustment (GIA) and other geological and hydrological processes (Boon et al., 2010; Kopp, 2013; Miller et al., 2013), but the GIA impact has a time-scale of thousands of years, which is distinguishable from shorter-term ocean dynamics-driven variability studied here. The spatial pattern of this hotspot is consistent with dynamic sea level changes that have been seen in different numerical ocean models (Ezer, 1999, 2001; Levermann et al., 2005; Yin et al., 2009; Yin and Goddard, 2013; Griffies et al., 2014; Goddard et al., 2015). However, the regional pattern of sea level anomaly associated with changes in AMOC may be complicated and depends on the time scales of interest; there is a clear sea level response pattern near the GS due to interannual changes, but much broader spatial response of sea level to multidecadal variations (Lorbacher et al., 2010). Therefore, the study will use an analysis method that separates oscillations on different time scales.

Because of the sea level gradient across the GS (i.e., sea level is lower/higher on the onshore/offshore side of the GS), changes in the path and strength of the GS are expected to impact coastal sea level variations along the U.S. East coast; this idea is behind the main motivation of our study to estimate changes in offshore ocean currents from coastal

* Tel.: +1 757 683 5631.
E-mail address: tezer@odu.edu.

http://dx.doi.org/10.1016/j.gloplacha.2015.03.002
0921-8181/

tide gauge measurements. Over the years, several studies found significant correlations between variations in the GS and coastal sea level (Blaha, 1984; Ezer, 2001, 2013; Sweet et al., 2009; Ezer et al., 2013; Ezer and Atkinson, 2014), suggesting that the recent SLR acceleration may be driven by weakening AMOC and the GS (Sallenger et al., 2012; Ezer et al., 2013). However, the mechanism in which large-scale changes in ocean circulation affect the pattern of coastal sea level rise is complex, as it involves several processes such as changes in the southward flowing coastal slope current (Rossby et al., 2010), wind-driven changes in the GS and the Subtropical Gyre (Zhao and Johns, 2014), wind forcing on the shelf (Woodworth et al., 2014), climatic change in subpolar regions (Hakkinen and Rhines, 2004) and vertical divergence of large-scale ocean currents (Thompson and Mitchum, 2014). Some of these processes, as well as changes in the North Atlantic Oscillations (NAO) contribute to changes in the Atlantic Meridional Overturning Circulation (AMOC; McCarthy et al., 2012; Srokosz et al., 2012; Smeed et al., 2013). The GS, as part of the upper branch of the AMOC, may serve as a mean to transfer signals originated by climatic changes in the open ocean far away from coasts, into signals that can be detected at the coast — a recent example is the extreme sea level anomaly observed along the U.S. northeastern coast in 2009–2010 (Sweet et al., 2009; Goddard et al., 2015). Therefore, three elements are studied here and compared, AMOC, GS and sea level. The possibility of detecting changes in AMOC and the GS from sea level data is especially intriguing, given that from the 3 elements, only sea level had been continuously measured for more than a century.

While a weakening in the AMOC under warmer climate conditions is expected (Hakkinen and Rhines, 2004; Lorbacher et al., 2010; McCarthy et al., 2012; Sallenger et al., 2012; Srokosz et al., 2012; Smeed et al., 2013), there is ongoing debate whether or not this change can be detected from past observations. Continuous direct observations of all the components contributing to the AMOC transport are available from the RAPID project for only ~10 yrs, since 2004 (McCarthy et al., 2012; Srokosz et al., 2012; Baringer et al., 2013; Smeed et al., 2013), so they cannot resolve decadal or multidecadal variations which dominate the Atlantic Ocean dynamics (Sturges and Hong, 1995, 2001; Ezer, 1999, 2001, 2013; Rossby et al., 2014). Various attempts have been made to reconstruct the variations of AMOC in the past, for example, using sea surface temperature (SST) data (Klöwer et al., 2014), which captures the heat flux-driven part of AMOC. A different approach is proposed here, using observations of sea level difference across the GS. Observations of the GS flow by the Oleander container ship (Rossby et al., 2010, 2014) and by altimeter data (Ezer et al., 2013) span ~20 yrs and observations of the Florida Current (FC) at the Florida Strait (Baringer et al., 2013) span ~30 yrs of data. However, all the above data records are still short relative to the ~60-year cycle that may be associated with the Atlantic Multidecadal Osillations (AMO) (Chambers et al., 2012). Sea level data from tide gauges (Woodworth and Player, 2003; Church and White, 2011; Woodworth et al., 2014) have been monitored at a much higher rate (as frequent as hourly or daily) and have been recorded for much longer periods (in some locations over 100 yrs) than the AMOC or GS observations, so these data will be used here to reconstruct a longer proxy of the AMOC record. However, even in the long sea level records, decadal and multidecadal variations make the detection of long-term acceleration or identifying the sources of changes in trends difficult (Haigh et al., 2014).

Because of the different lengths of the records and the different instrumentations used, as mentioned above, there are sometimes discrepancies between different studies of the GS which may create confusion. For example, Rossby et al. (2014) claim that the Oleander data does not provide evidence that the GS is slowing down, a claim that appears to contradict evidence from other data showing recent slowing down of the GS (Sallenger et al., 2012; Ezer, 2013; Ezer et al., 2013) and weakening AMOC (Smeed et al., 2013). However, a close examination here will show that there is no real contradiction between different data sources. On the one hand, Rossby et al. (2014) looked at the average linear trend of the upper GS flow over 20 yrs, which indicates a small downward trend that is not statistically significant at 95% confidence level given the large variability in the GS flow. On the other hand, Sallenger et al. (2012) and Ezer et al. (2013) looked at non-linear changes, indicating that weakening of the GS and AMOC is not constant, but may have accelerated in recent years (Ezer et al., 2013, noticed a particular faster decline in the GS strength after ~2004). There is no reason to expect that climate trends will continue at the same rate over long period of time, so one has to look at the variability, not just the long-term mean trend; this is one of the goals of this study.

Comparing the variations and trends in different data sets is not a straight forward task when observations use different instruments, different sampling intervals and different locations (Fig. 1). For example, defining the upper GS flux and front position in the Oleander section between Bermuda and the U.S. coast (Rossby et al., 2014) is a complex task, as seen in Fig. 1. The GS is meandering, the flow field includes

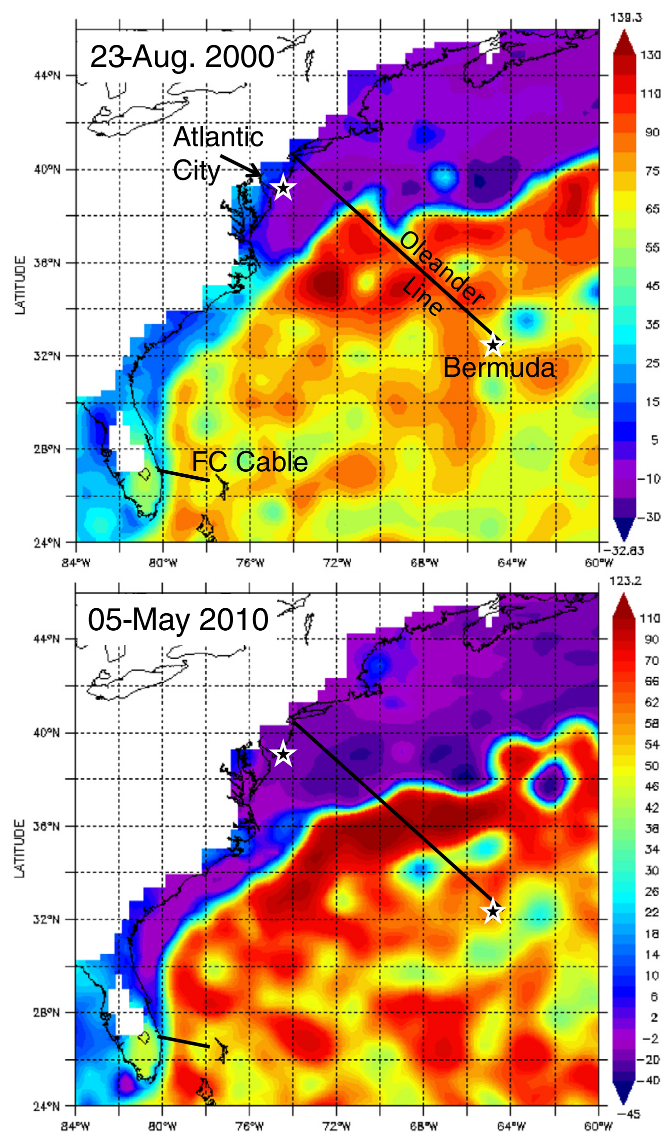

Fig. 1. Examples of absolute sea surface height (cm; in color) from altimeter data. Top: August 23, 2000, when the Gulf Stream front was farther north. Bottom: May 5, 2010, when the Gulf Stream front was farther south. Also shown are approximated locations of data used in the study: the Oleander section, the Florida Current section and the tide gauges (marked as stars). (For interpretation of the references to color in this figure legend, the reader is referred to the web version of this article.)

recirculation gyres and eddies, and potential deep return flows may not be captured by observations of the upper layers. On the other hand, the RAPID data set (McCarthy et al., 2012), uses the observed FC transport upstream to represent the GS portion of the AMOC. The FC is a measure of the total flow in a relatively shallow channel, and it is influenced by variability associated with wind-driven subtropical gyre circulation. Therefore, one must keep in mind the distinction between what is defined as "GS" in the Oleander data and in the RAPID data. The FC and the GS at the two sections (Fig. 1) are however related to each other — in particular, a coherent wind-driven variability along the length of the GS has been seen in data and models (Zhao and Johns, 2014). An attempt will thus be made here to see which portion of the AMOC is correlated with which part of the Oleander section.

The RAPID data show two interesting phenomena, a general decline in the AMOC transport since 2004 that is largely due to changes in the geostrophic part of AMOC (Smeed et al., 2013) and a much larger decline, by as much as 30% in the AMOC transport in 2009–2010 that is largely driven by changes in the Ekman transport during a period of intense negative NAO (McCarthy et al., 2012). The extreme AMOC drop in 2009–2010 seems to be the cause of anomalously high water levels along the northeastern coast of the U.S. (Goddard et al., 2015) and increase in flooding during this time (Sweet et al., 2009; Ezer and Atkinson, 2014). Based on climate models, Roberts et al. (2014) suggest that the general AMOC decline was not inconsistent with low-frequency variability in the models, so a much longer observed AMOC record is needed to know how unusual the 2009–2010 event was. On the other hand, the sea level response detected north of New York City in 2009–2010 was extremely rare according to Goddard et al. (2015).

It is interesting to note that based on past temperature and salinity observations, diagnostic numerical ocean models suggest that a dramatic decline of ~30% in the GS transport happened between the 1960s and 1970s, which resulted in 5–10 cm increase in sea level along the U.S. east coast (Greatbatch et al., 1991; Ezer et al., 1995). At the time there were no direct observations of AMOC or altimeter data of the GS, as exist today, so there was no way to verify if those model-based findings are real or not. However, the close resemblance of the past changes to recent changes in AMOC and sea level motivated an attempt here to compare the recent AMOC changes with other long-running observations, and put them into context with past changes.

The above uncertainties motivated this study and prompted three goals. First, a comparison between different data sets of the GS and AMOC using similar averaging periods is conducted in order to reveal if there are discrepancies between the data sets. Second, the different components of the AMOC transport (i.e., Ekman transport, mid-ocean transport and Florida Current transport; McCarthy et al., 2012) and the different components of the Oleander sections across the GS (Slope Current, Gulf Stream and Sargasso Sea; Rossby et al., 2010) are compared in order to study forcing mechanisms and their relations. Third, the relatively short AMOC observations are combined with the longer sea level data to reconstruct a proxy for AMOC transport over the past ~80 yrs, in order to study the AMOC variability, trends, and potential climate-related changes. This reconstruction follows on the footsteps of Ezer (2013) who found very significant correlations between the AMOC transport and the sea level difference between Bermuda and the U.S. coast (i.e., across the GS). The analysis method used here include Empirical Mode Decomposition/Hilbert–Huang transform (EMD/HHT; Huang et al., 1998), which is a non-parametric method that can separate oscillating modes from non-linear trends in time series that may include non-stationary components (e.g., oscillations with time-dependent frequency). The EMD/HHT has been used in the past for various applications, from seismic signals and physics to economics data, but only quite recently the method has been adapted for studies of climate change and sea level rise trends (Ezer and Corlett, 2012; Ezer, 2013; Ezer et al., 2013).

2. Data analysis and comparisons

2.1. Coastal sea level data and the Gulf Stream obtained from the Oleander measurements

Monthly mean sea level records are obtained from the Permanent service for Mean Sea Level (PSMSL; Woodworth and Player, 2003). The relative coastal sea levels for most of the stations along the entire U.S. East Coast have been analyzed in details — they show a distinct regional pattern suggesting an ocean dynamic influence (Ezer, 2013), as discussed before. Here, the records of 2 stations are used, Atlantic City and Bermuda, for the period 1935–2012; the locations of these stations are close to the end points of the Oleander sections (Fig. 1), providing sea levels in opposite sides of the GS. Gaps in the Bermuda record during the 1940s and 2000s were filled with linear interpolation; these gaps have no significant impact on the overall trends and variability. Fig. 2a shows that the two stations have somewhat different interannual variations and linear trends. The SLR in Atlantic City (4.1 mm yr^{-1}) is larger than that in Bermuda (2.4 mm yr^{-1}), whereas the value of global SLR from altimeter data (~3.2 mm yr^{-1}; Ezer, 2013) is between these two

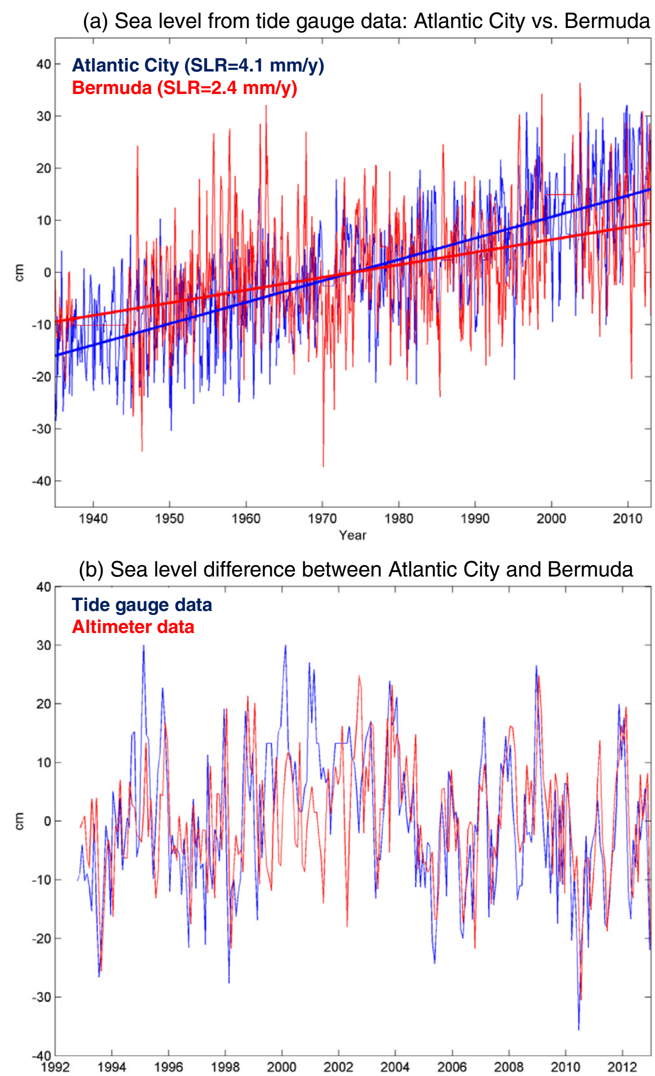

Fig. 2. (a) Monthly sea level data and linear trends from tide gauges in Atlantic City (blue) and Bermuda (red). (b) Sea level difference (Bermuda minus Atlantic City) obtained from coastal tide gauges (blue) and from altimeter data (red). Altimeter data are from ocean locations closest to the tide gauges. (For interpretation of the references to color in this figure legend, the reader is referred to the web version of this article.)

values. The land subsidence in Atlantic City (mainly GIA-related) is estimated to be ~1 mm yr^{-1}, and larger than land subsidence in Bermuda (Kopp, 2013; Miller et al., 2013), so the remaining difference, $4.1 - 2.4 - 1.0 = 0.7$ mm yr^{-1} may suggest some small decline in the slope across the GS, though given the uncertainties in the SLR trends (± 0.2 mm yr^{-1}) and in land subsidence (± 0.5 mm yr^{-1}) this long-term change is not statistically significant. Interannual and decadal variations in sea level difference are large and statistically significant relative to the long-term mean or trend. Gridded altimeter data are obtained for 1993–2012 from the AVISO site (www.aviso.altimetry.fr), and examples of absolute sea surface height fields are shown in Fig. 1. Fig. 2b shows the monthly sea level difference (SLDIF) between Atlantic City and Bermuda, calculated from the tide gauges and from altimeter data (the closest points to the tide gauges, within ~25 km). Except a distinct period around 2000–2002, there is a good agreement between the tide gauge and altimeter data (overall correlation R = 0.8 with statistical significance confidence C = 99.9%), which is somewhat surprising, given that near-shore processes such as coastal currents, upwelling events and storm surges are not captured by the altimeter data that well. Therefore one may conclude that the SLDIF record represents interannual and decadal variations in the slope across the GS, and in fact, Fig. 2a resembles the variations of the GS strength shown in Ezer et al. (2013). Note that the SLDIF shows a large decline of ~0.5 m between a maximum slope in 2009 and a record minimum in 2010. For an average sea level difference across the GS of ~1.5 m (Ezer et al., 2013) this change represents ~30% decline in geostrophic flow, which is comparable to the 30% drop in AMOC in 2009–2010 (McCarthy et al., 2012) and coincides with unprecedented sea level rise on the U.S. coast at that time (Goddard et al., 2015).

The Oleander observations to monitor the GS are described in Rossby et al. (2010, 2014) and were obtained for 1993–2012. These observations of the upper ocean are taken by Acoustic Doppler Current Profiler (ADCP) mounted on a container vessel (CMV Oleander) that operates weekly between New Jersey and Bermuda (intervals are irregular with a notable large gap in 2010). Current profiles have been taken down to a depth of ~200–300 m until 2004 and ~500–600 m since 2005. The lines are divided into three subsections from north-west to south-east: (1) The "Slope Current", from 39.31°N, 72.57°W to the northern limit of the GS; (2) the "Gulf Stream", which is bounded by where the velocity normal to the ship's track goes to zero from either side; and (3) the "Sargasso Sea", from the southern limit of the GS to 32.78°N, 64.89°W. Data are in units of fluxes (m^2 s^{-1}) representing mean upper layer transport for a 1-m thick layer. Averages over a 12-month window at six month intervals and their 95% confidence error bars are provided by the University of Rhode Island (see Rossby et al., 2014, for details). The GS position for each section is calculated from the maximum GS speed. The time variations in the total Oleander section flux and the three parts mentioned above are shown in Fig. 3a, d, e, and f, and the GS position is shown in Fig. 3c. Also shown in Fig. 3b is the SLDIF anomaly from the tide gauges, now calculated on exactly the same 6-month interval periods when the Oleander data are available. Note that error bars are the 95% confidence intervals relative to the 12-month mean values — they represent a measure of the variability within the 12-month window, not any observed or analysis errors. One should keep in mind that for the limited record length of the data used here a single extreme event such as the peak seen in 2010 can have a large influence on the statistics. Note the clear compensation between the different parts of the flow, for example, in 2010 an extreme high peak in the GS (Fig. 3d) is balanced by extreme negative Sargasso Sea flow (Fig. 3f); unfortunately, there are gaps in the measurements during this time. Note the statistically significant positive correlation between SLDIF (Fig. 3b) and the total Oleander flux (R = 0.46; Fig. 3a). However, somewhat surprisingly, there is no statistically significant correlation between the GS part of the Oleander line and SLDIF (R = −0.22; not statistically significant at 95%); this GS flow is the part of the Oleander line in Rossby et al. (2014) that did not show the weakening trend found in other data. The SLDIF is significantly correlated with the GS position (R = 0.49), whereas the GS takes a position closer to shore (as in top of Fig. 1) when the total sea level slope is larger and vise versa. Of particular curiosity is the sudden northward shift in the GS, by as much as 150 km, around 2000 that followed by a gradual southward return during 2000–2010, when at the same time the total flux and SLDIF gradually weakened; this southward shift in the GS between 2000 and 2011 has been previously indicated by Ezer et al. (2013) and also involved a weakening in the GS and acceleration in coastal SLR. The correlations between SLDIF and the Oleander data are summarized in the left column of Table 1.

2.2. Comparison of Gulf Stream measurements versus AMOC

The AMOC data is based on the RAPID observations at 26.5°N for 2004–2012, as described in recent studies (McCarthy et al., 2012; Srokosz et al., 2012; Baringer et al., 2013; Smeed et al., 2013). The total AMOC transport (given in Sverdrup; 1 Sv = 10^6 m^3 s^{-1}) is the sum of three components: (1) The Florida Current transport measured by the cable across the Florida Strait; (2) the Ekman transport estimated from wind stress; and (3) the mid-ocean transport calculated from observations of density changes across the Atlantic Ocean. Although the data is provided in 12-hourly intervals, only monthly averages will be used here for consistency with the sea level data.

The definitions of the components of the RAPID observations and the components of the Oleander observations are different, so one must verify what each component means and how it relates to other components. The correlations associated with the Oleander observations for 1993–2012 are summarized in Table 1 and the correlations associated with the RAPID observations are summarized in Table 2. The main findings on the relation between the AMOC and the Oleander data are shown in Fig. 4. First, it is somewhat surprising that the "Oleander's Gulf Stream" is not correlated with any of the AMOC components (second column in Table 2), even slightly anti-correlated (though not at a statistically significant level) with the FC upstream from the OGS. This result is in contrast with the significant correlation found between the FC and the GS flow derived from altimeter data averaged over the mid-Atlantic region (Ezer et al., 2013). This finding of no correlation between OGS and FC may explain why Rossby et al. (2014) could not find significant weakening trend in the OGS that is consistent with the GS and AMOC weakening seen in other data (Ezer et al., 2013; Smeed et al., 2013). It seems that the OGS along a single line is dominated by the influence of eddies, meandering and recirculation in the Sargasso Sea (Gulf Stream–Sargasso Sea correlation, R = −0.6; Table 1), as noted by Rossby et al. (2010, 2014). Therefore, the OGS seems to represent local dynamics more than it represents the total transport changes associated with AMOC. On the other hand, the total flow across the entire Oleander line (including all 3 components) is a good representation of the total AMOC transport (R = 0.67), and both show weakening transport between 2006 and 2010 (Fig. 4a). Another interesting result is that unlike the OGS flow which is uncorrelated with the FC, the location of the GS front along the Oleander line is anti-correlated with the FC transport upstream (R = −0.65; Fig. 4b). The fact that a stronger GS implies a southward shift in the GS upstream of Cape Hatteras on interannual time scales (Fig. 4b) is consistent with similar pattern found in decadal variations during the period 1950–1990 (see Fig. 7 in Ezer, 1999); these types of long-term variations have been suggested in the past to be associated with baroclinic Rossby waves propagating across the North Atlantic basin (Sturges and Hong, 1995; Ezer, 1999). While the Oleander's Slope Current (OSC in Table 2) is not statistically correlated (at over 95% confidence) with AMOC, altimeter data show that a stronger slope current can be developed when the GS shifts away from the coast, as is the case between 2000 and 2011 (Ezer et al., 2013); this relation is consistent with simple dynamics of opposing currents, and with previous studies (e.g., Joyce et al., 2000) that related a southward shift in the GS position to low NAO index, and to a stronger

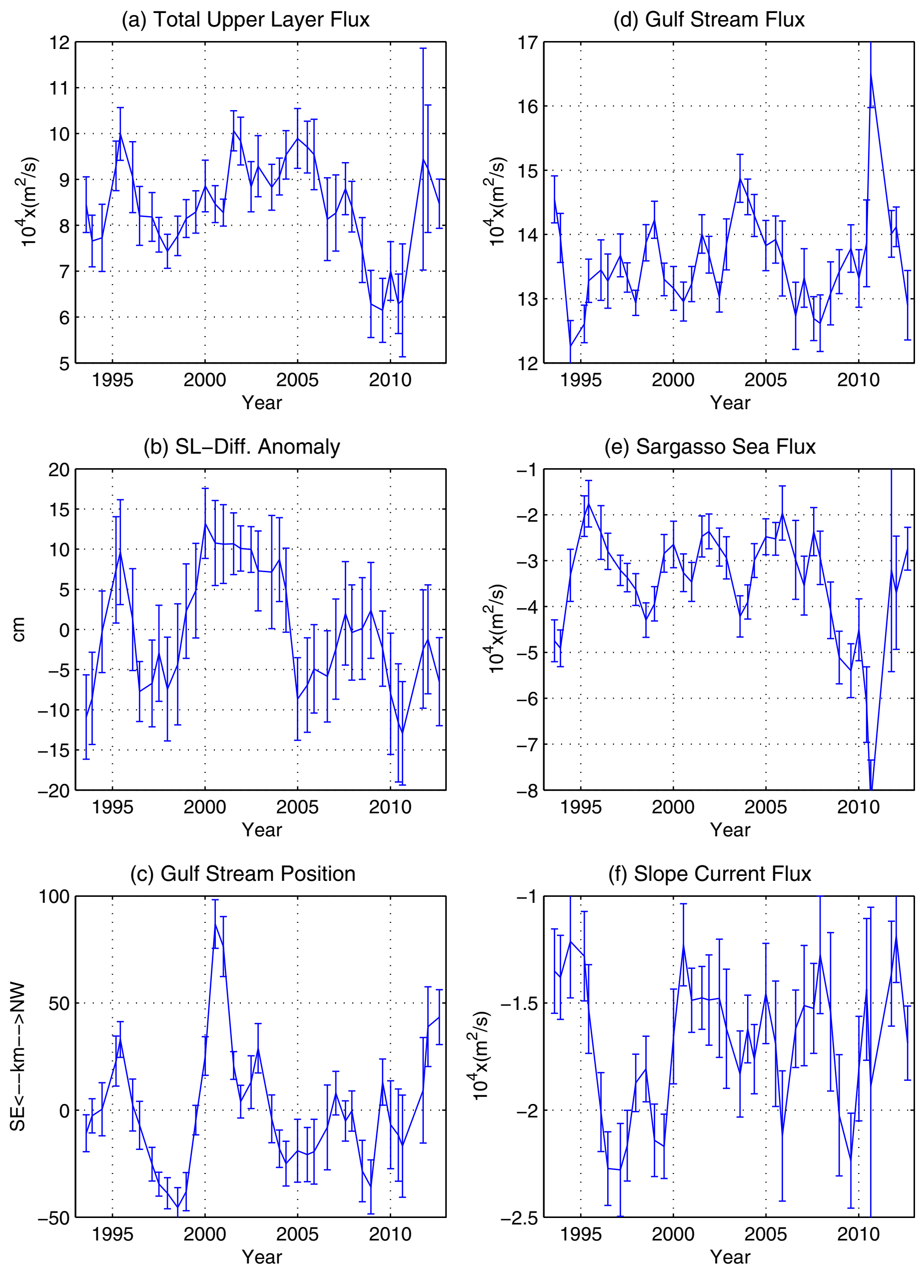

Fig. 3. Section data between Bermuda and the U.S. coast obtained from the Oleander project and from tide gauge data (only panel b). All data are annual averages and error bars (vertical lines) representing 95% confidence intervals relative to 12-month means; some data were missing in 2011. (a) Total volume flux of the upper layers across the entire section (in 10^4 m^2 s^{-1}) and its components: (d) the Gulf Stream portion of the section, (e) the Sargasso Sea portion, and (f) the Slope Current portion; (c) is the Gulf Stream relative location on the Oleander section (in km; with positive values toward the U. S. coast; see Rossby et al., 2014, for details). (b) Bermuda–Atlantic City sea level difference anomaly (in cm).

Table 1
Correlation coefficients between the fluxes measured by the Oleander project during 1993–2012 and sea level difference (SLDIF) between Bermuda and Atlantic City. The calculations are based on 12-month averages in 0.5 year intervals at periods when Oleander data are available. Correlations with confidence level C > 95% are highlighted in bold.

	Sea-level difference	Oleander fluxes		
	SLDIF	OGS	OSC	OSS
Oleander's Total Flux (OTF)	**0.46**	−0.06	0.31	**0.8**
Oleander's Gulf Stream (OGS)	−0.22	1	−0.19	**−0.6**
Oleander's Slope Current (OSC)	0.21	−0.19	1	0.12
Oleander's Sargasso Sea (OSS)	**0.47**	**−0.6**	0.12	1
Oleander's GS Position (OPO)	**0.49**	−0.24	**0.48**	0.26

AMOC (Joyce and Zhang, 2010). All these findings seem to suggest that the Slope Current by itself is not a significant driver of variations in the GS position, but perhaps a result of several processes, including the location of the GS and the supply of source waters from the Labrador Sea and the subpolar gyre. Contributions to the Sargasso Sea portion of the Oleander line seem to come mostly from the mid-ocean portion of the AMOC ($R = 0.53$; Fig. 4c), resulting in strong connections with the total AMOC transport ($R = 0.65$). Note that the Sargasso Sea flow seems to lag behind the AMOC signal.

2.3. The 2009–2010 AMOC weakening: comparisons of three independent data sets

The weakening trend in the AMOC transport between 2004 and 2012 (~−0.5 Sv per year; Smeed et al., 2013) and the dramatic decline

Table 2
Same as Table 1, but for correlations between the Oleander fluxes and the AMOC transports during 2004–2012. Correlations with confidence level C > 95% are highlighted in bold.

	Oleander's fluxes				GS position (OPO)
	Total (OTF)	Gulf Stream (OGS)	Slope Current (OSC)	Sargasso Sea (OSS)	
AMOC's Total Transport (ATOT)	**0.67**	−0.24	0.18	**0.65**	−0.32
Florida Current transport (AFCT)	0.12	−0.2	−0.37	0.26	**−0.65**
Ekman transport (AEKT)	0.38	−0.27	0.29	0.4	0.19
Mid-ocean transport (AMOT)	**0.64**	−0.1	0.24	**0.53**	−0.26

in 2009–2010 (McCarthy et al., 2012; Srokosz et al., 2012; Baringer et al., 2013) are intriguing, though separating trends from internal variability may require much longer records (Roberts et al., 2014). In some contrast to the above findings of significant recent changes in ocean circulation, Rossby et al. (2014) claim that the GS remained relatively stable over the past 20 yrs. This claim is based on the Oleander observations across the GS over a period longer than the RAPID data. Therefore, to see if the different data sets are consistent with each other, 3 independently obtained records are compared in Fig. 5: (a) the Oleander total transport (blue line); (b) the SLDIF (red line); and (c) the AMOC total transport (green line); the 12-month average values and error bars at 6-month intervals are plotted at exactly the

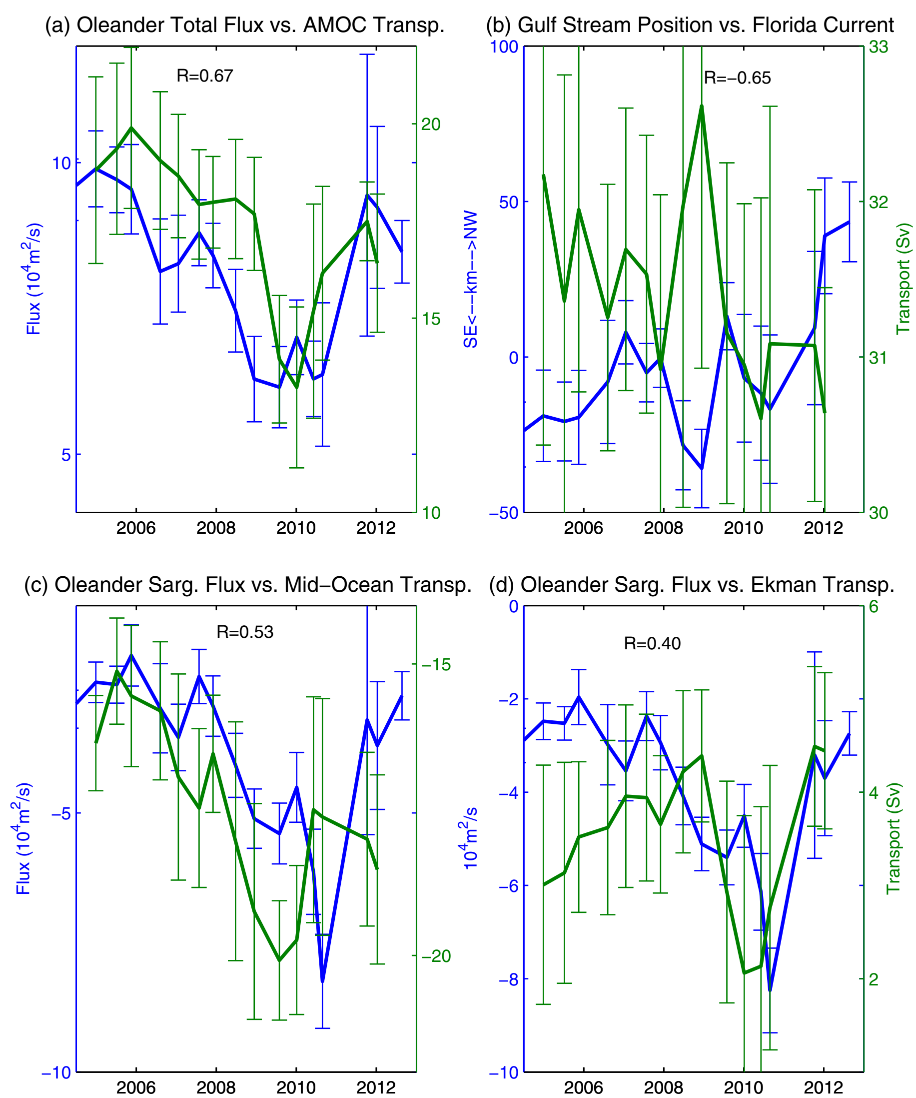

Fig. 4. Comparisons between the Oleander observations (blue lines and y-axis on the left; same units as in Fig. 3) and the RAPID transport data (green lines and y-axis on the right; units are Sv). Annual means and errors in ~0.5 year intervals are shown for periods when Oleander data are available (note gaps in data during 2011). (a) Total flux across the entire Oleander section vs. total AMOC transport. (b) Gulf Stream position vs. Florida Current portion of AMOC. Sargasso Sea portion of Oleander line is shown vs. (c) mid-ocean and (d) Ekman transport portions of AMOC. (For interpretation of the references to color in this figure legend, the reader is referred to the web version of this article.)

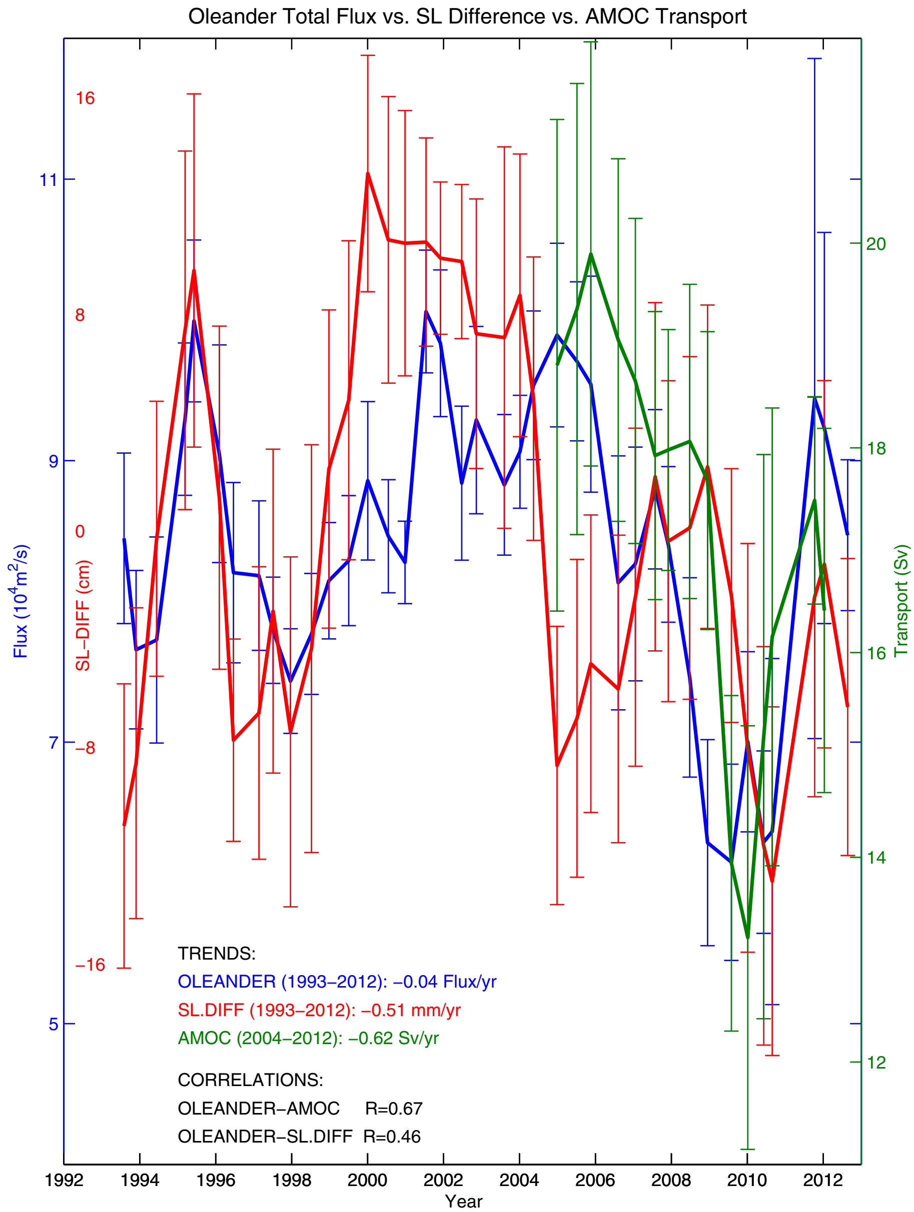

Fig. 5. Comparisons between 3 different data sets: Oleander total flux (blue line; y-axis on outside-left), sea-level difference (red line; y-axis on inside-left) and AMOC transport (green line; y-axis on right). Data and units are the same as in Figs. 3 and 4. Various trends and correlations are indicated. (For interpretation of the references to color in this figure legend, the reader is referred to the web version of this article.)

same points in time when all data are available. Note that (a) and (b) represent integrated values across the same line (located ~32°N–40°N), while (c) represents transport across 26.5°N. Though the 3 data sets differ by the period covered, by the units used, and by the property they measure (though all represent a property associated with the Atlantic circulation strength), the variations are strikingly similar. When compared on the same intervals, the Oleander data is significantly correlated with AMOC ($R = 0.67$) and with SLDIF ($R = 0.46$). All three data sets show that the weakest flow occurred in 2010, but the downward trend may have started around 2000 (before the start of the RAPID project); the unusual drop in AMOC in 2009–2010 (McCarthy et al., 2012; Goddard et al., 2015) is the last part of this trend. Some discrepancy between SLDIF and the other two data sets is seen in 2005, which may relate to unknown coastal processes not captured by the Oleander and RAPID observations. Even before the RAPID program started, the variations in the Oleander-measured flow and SLDIF are very similar. All the records have downward trends over 1993–2012 and 2004–2012. These trends will be evaluated later with respect to a much longer reconstructed record to evaluate if the trend over the past decade or so is unusual or not. Note that the conclusion of Rossby et al. (2014) about a stable Gulf Stream, with large variability and no significant trend, was based on only a portion of the Oleander line (OGS) which is affected by eddies more than by AMOC and does not address the trend during the RAPID period. The main point here is that the 3 data sets are generally consistent with each other and the apparent discrepancy in different studies one may mistakenly infer from Rossby et al. (2014) reflects the fact that the studies look at different periods and only part of the data (i.e., subsection OGS rather than the whole section).

3. AMOC and sea level variability based on Empirical Mode Decomposition

To better understand the relation between variations in AMOC and SLDIF, an Empirical Mode Decomposition/Hilbert–Huang transform (EMD/HHT; Huang et al., 1998) method is used, as in previous studies of sea level records (Ezer and Corlett, 2012; Ezer, 2013; Ezer et al., 2013). The non-parametric, non-stationary, method can separate oscillating modes from non-linear trends, so the SLDIF record (SL) and the AMOC transport record (TR) are represented by:

$$\mathrm{SL}(t) = \sum_{i=1}^{N} c_i(t) + r(t) \tag{1a}$$

$$\mathrm{TR}(t) = \sum_{i=1}^{N} d_i(t) + s(t) \tag{1b}$$

where c and d are intrinsic oscillating modes and r and s are residual trends, for SLDIF and AMOC transport, respectively. If the 2 time series have similar length and variability, the number of modes, N, is likely to be the same, as is the case here (for monthly data 2004–2012, $N = 5$ oscillating modes; $N = 0$ is defined as the original data and the trend, r or s, are also referred to as mode 6). The definition of the trend in the EMD calculation is "a time-dependent function with at most one extremum representing either a mean trend or a constant" (Wu et al., 2007). Using linear regression, one can correlate the modes in each data set, whereas modes and trends of AMOC can be predicted from the SLDIF modes by:

$$d_i(t) = a_i c_i(t) + b_i \tag{2a}$$

$$s(t) = a r(t) + b \tag{2b}$$

where a's and b's are the regression coefficients. The EMD analysis is an empirical, sifting, non-linear approach, applied to non-stationary time series, so studies use various statistical methods to estimate confidence levels in the EMD analysis. For example, Huang et al. (2003) used variations in the sifting parameters to obtain confidence intervals, Ezer and Corlett (2012) used bootstrap simulations, and recently Kenigson and Han (2014) used artificially constructed time series to evaluate the accuracy of detecting trends. In the approach presented here, first, a standard EMD is applied, and then an Ensemble EMD (EEMD) with an added random white noise (Wu and Huang, 2009) was used to evaluate the statistics, errors and robustness of the analysis.

Fig. 6 compares the EMD modes in AMOC and SLDIF (with 2-month lag added; SLDIF is downstream from the FC thus lags behind AMOC) and also shows the cross-correlation function for each mode (right panels). The first two high frequency modes with periods less than 1 yr are not well correlated and not shown, but significant correlations are evident for most other modes. Modes 3, 4 and 5 represent oscillations of ~1, ~2 and ~5 year periods, respectively. Of particular high correlations are mode 4 ($R = 0.81$), which together with mode 5 represents the weakening AMOC in 2010 discussed before, and mode 6, the trend ($R = 0.99$). The almost identical EMD trends in both AMOC and SL show a nonlinear trend with increased slope in recent years, but it is likely affected by unresolved multidecadal variations, as shown later. Because of the filtering of the high-frequency modes it is not a straight forward task to evaluate the significance of the extremely high correlations of the low-frequency EMD modes. Therefore, ensemble calculations (EEMD) are used to evaluate the robustness of the analysis of the low-frequency variations (modes 4 + 5 + 6; Fig. 7). The EEMD performs 100 EMD calculations for each data set, with a random white noise of 15% added to each calculation (representing potential data errors). If a particular set of modes is robust, the ensemble mean will converge and the standard deviation will show how errors vary along the time series and how significant are peaks relative to potential errors. It appears that the analysis has larger errors (spread of the ensemble members) near the beginning and the end of the records, but the SLDIF represents very well the 2009–2010 event (Fig. 7). The high correlation of the low-frequency modes of SLDIF and AMOC ($R = 0.74$, $C = 99.9\%$) is mostly due to the similar representation of the 2009–2010 event in the two data sets. This correlation is obtained with a 5-month lag (SLDIF lags behind AMOC) which is consistent with the fact that the SLDIF line is located downstream from the FC and the RAPID observations. Note that the existence of lag suggests that real-time measurements of AMOC may be useful as a potential predictor for changes in sea level. Another result from the EEMD test is that, of the 100 calculations (both in SLDIF and in AMOC) none had as low value as in the minimum in 2010 (neglecting the edges of the records), indicating the uniqueness of this event in a more statistical sense than a single calculation.

To further evaluate what processes that are included in the AMOC record are detected by the SLDIF, Fig. 8 compares the SLDIF with each one of the 3 components that make the AMOC transport. The Ekman transport seems to be significantly correlated with SLDIF at all frequencies (Fig. 8a, d, g), indicating that the wind-driven contribution to SLDIF affects a wide range of time-scales. However, the FC transport is highly correlated ($R = 0.89$, $C = 99.9\%$) with a 5-year cycle of SLDIF (Fig. 8e), but not at other cycles. The trend in both, the FC and SL are downward over the entire period, but the non-linear trend is in opposite phase (Fig. 8h), indicating possible compensation between FC and the other two components of AMOC on very long time scales. The most apparent feature in the low frequency modes of the mid-ocean part of AMOC is that it lags behind the SLDIF and the Ekman transport by about 2 yrs, suggesting that it may be driven by large scale changes in wind pattern, and it is not a driver of other components. The minimum AMOC transport in 2010 (discussed before) is detected by EMD mode-4; this mode shows minimum in both, the Ekman transport (Fig. 8a) and FC transport (Fig. 8b) at the same time that a minimum in SLDIF is seen. This result is consistent with previous studies that point to negative NAO and related changes in wind-driven Ekman transport as important contributors to the 2009–2010 event, but here it was shown that sea level can also detect this change in transport.

4. Reconstruction of an AMOC proxy for 1935–2012 from sea level data

The correlation found here between the observed SLDIF and the AMOC transport for 2004–2012 suggests that SLDIF may represent some of the AMOC variability, in particular, the wind-driven component of AMOC and interannual variations such as the 2009–2010 anomaly are detected quite well by SLDIF. Model simulations were also examined. For example, the correlation between SLDIF (Bermuda to U.S. coast) and the AMOC transport simulated by NEMO (Nucleus for European Modelling of the Ocean; not shown) indicates very similar correlations and lags as those found in the observations. The NEMO model simulations are those used by Blaker et al. (2014) for 1958–2001, which show past anomalies (e.g., in 1969/70) resembling the observed anomaly of 2009/10. The findings here add to past studies that found connections between large scale Atlantic Ocean transports and coastal sea level (Greatbatch et al., 1991; Ezer et al, 1995; Sturges and Hong, 1995; Ezer, 1999, 2001). Because of the relatively short period of continuous AMOC measurements by the RAPID project, any efforts to evaluate the accuracy of reconstruction of past AMOC are quite limited and may have considerable errors, for example due to biases in ocean models (Klöwer et al., 2014). Estimation of variations in AMOC transport is done here by the regression between AMOC and SLDIF with 2-month lag (giving overall correlation of $R = 0.27$ at $C = 99\%$ confidence). Reconstruction using individual EMD modes with different lags will result in higher correlations than direct regression ($R = 0.5$, $C = 99.9\%$, for 2004–2012), but the accuracy for an extrapolation before 2004 is unknown, so only results using direct regression is shown here. It is recognized that only part of the AMOC variability is represented by the SLDIF-derived proxy, in particular, high-frequency variations may not be represented very well, but they are not the main focus here.

The AMOC transport is reconstructed for 1935–2012 (green line in Fig. 9) from the AMOC record of 2004–2012 (red line in Fig. 9) using the AMOC–SLDIF regression. The decadal and multidecadal variations

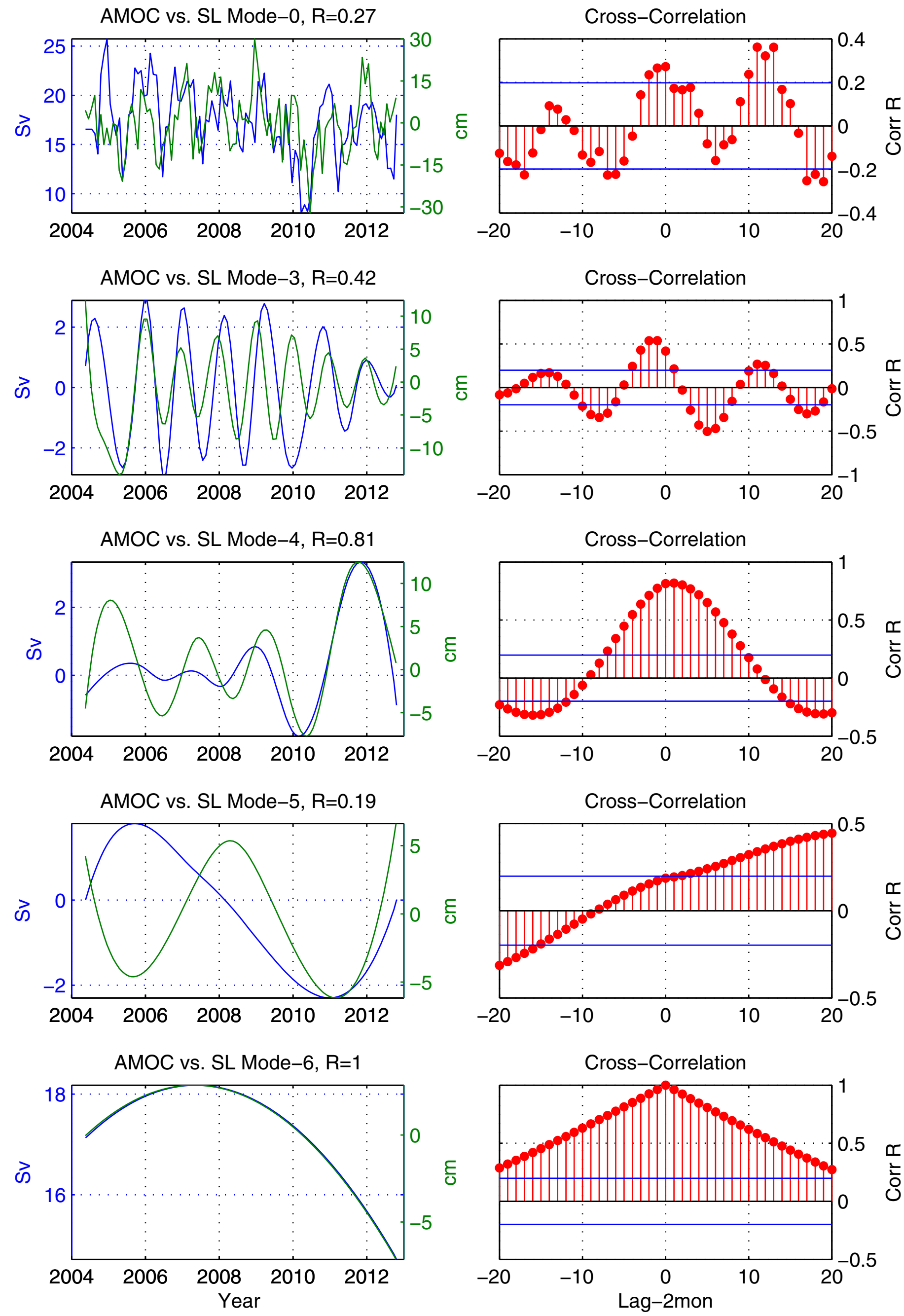

Fig. 6. Left panels are the EMD modes of the AMOC transport (in Sv; blue lines with axis on the left) and sea level difference (in cm; green lines with axis on the right). Right panels are the cross-correlations between sea level and AMOC data (blue horizontal lines are the 95% confidence intervals). The top panel is the original monthly data (mode 0), and below it are modes 3–6 from high to low frequencies (mode 6 is the long-term trend). The highest frequency modes 1–2 are not shown — sea level and AMOC are not well correlated in those modes. The frequency of each mode is not constant, but in general, modes 3, 4 and 5, represent oscillations with periods of 1, 2 and 5 yrs, respectively. (For interpretation of the references to color in this figure legend, the reader is referred to the web version of this article.)

obtained from the low frequency EMD modes are shown (black line in Fig. 9), as well as estimated transports from past observations (blue bars) reported by Bryden et al. (2005). The linear downward trend over the entire 78-year record is relatively small, −0.22 Sv per decade, and not statistically significant given the large variability and the uncertainty in sea level associated with land subsidence. However, qualitatively this weakening trend is consistent with Bryden et al. (2005). The record also shows interannual, decadal and multidecadal variability (periods of ~5, ~10 and ~50 yrs). The longer periods may include influence of the Atlantic Multidecadal Oscillations (AMO) (Chambers et al., 2012).

Attention was given recently to potential weakening in AMOC seen in the RAPID observations since 2004 and even a larger weakening of up to 30% during 2009–2010 (McCarthy et al., 2012; Srokosz et al., 2012; Baringer et al., 2013; Smeed et al., 2013), so it would be of interest to compare the recent large changes to past changes. In particular, several past studies focused on interpentadal changes that were detected in the Atlantic Ocean density field between 1955–1959 and 1970–1974 (Levitus, 1989), resulting in a reduction in steric sea level difference between the subtropic and the subarctic (Levitus, 1990), possibly a 30% decrease in the GS transport (Greatbatch et al., 1991) and ~10 cm sea

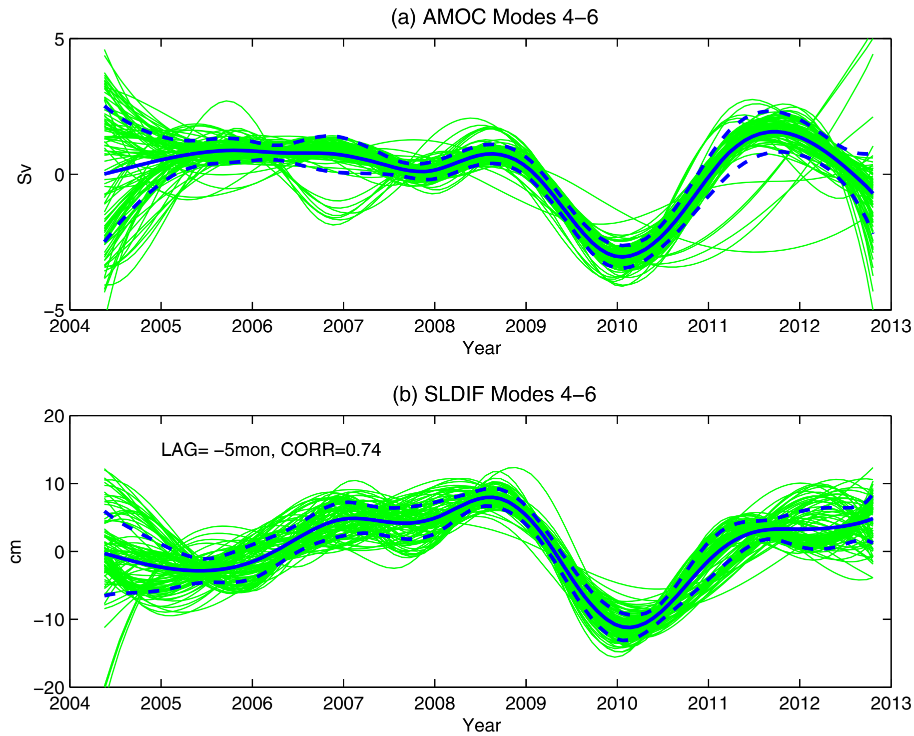

Fig. 7. Ensemble EMD (EEMD) calculations of the combined modes 4–6 using 100 ensemble members and random white noise equivalent to 15% of the observed standard deviation. Green lines are individual members and heavy blue lines are the ensemble mean (solid) and standard deviation (dash). (a) Monthly AMOC record and (b) monthly SLDIF record; the correlation coefficient with 5-month lag (AMOC leading SLDIF) is 0.74 (over 99.9% confidence level). (For interpretation of the references to color in this figure legend, the reader is referred to the web version of this article.)

level rise along the U.S. coast (Ezer et al., 1995). In comparison, during the 2009–2010 AMOC decline period sea level around New York city rose by ~13 cm (Goddard et al., 2015). The similarity between the changes observed in recent years and those observed in the 1960s and early 1970s suggest that a weakening in AMOC may have been involved in both cases. Both periods have been also characterized by negative NAO. The AMOC reconstruction indeed shows very similar transport decrease, ~4.5 Sv per decade for 1960–1972 and 2000–2012. Longer RAPID

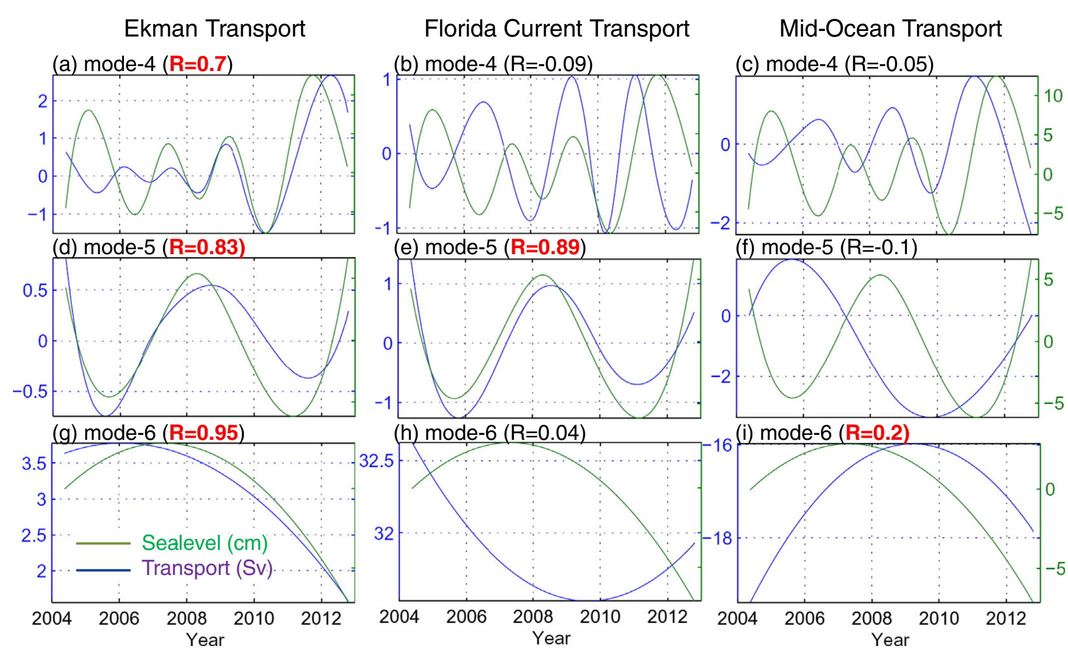

Fig. 8. The low-frequency EMD modes 4–6 (from top to bottom) of the three components of the AMOC transport (in Sv; blue lines with axis on the left) and sea level difference (in cm; green lines with axis on the right). Correlations (R) at 95% confidence and higher are highlighted in red. (For interpretation of the references to color in this figure legend, the reader is referred to the web version of this article.)

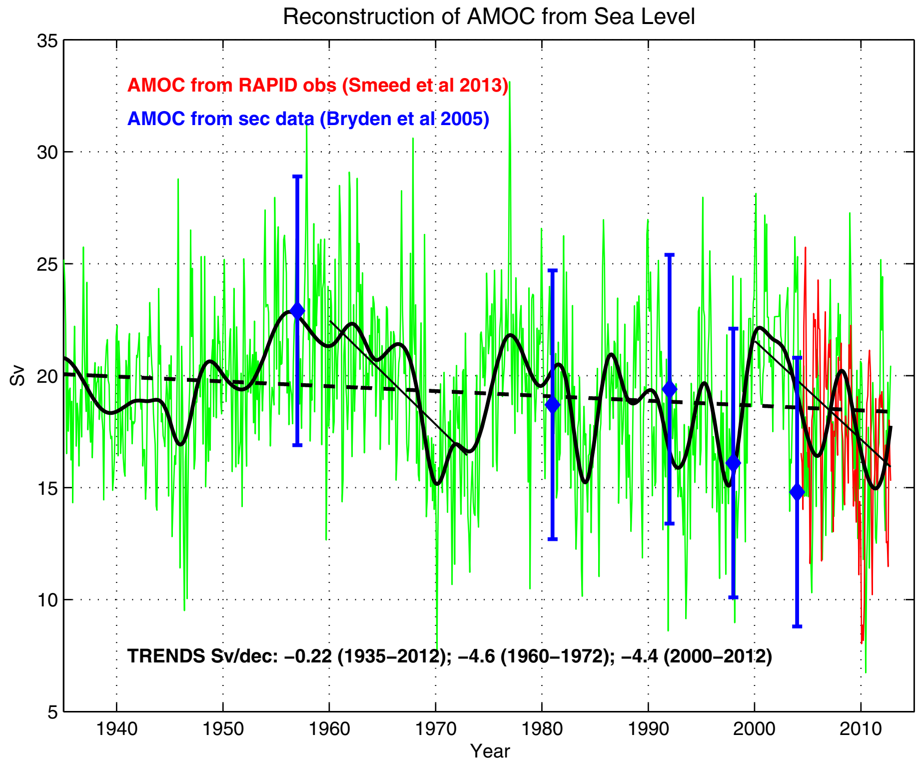

Fig. 9. Reconstruction of monthly AMOC record from 1935 (green line), using the correlation of sea level with observed AMOC after 2004 (red line). Blue lines represent estimated AMOC transport and error bars from section data across 25°N (Bryden et al., 2005). Also shown is the sum of the low-frequency EMD modes (heavy black line), the long-term linear trend line (dashed line) and the linear trend of two periods with especially large decline (thin black lines); the trends are indicated in Sv per decade. (For interpretation of the references to color in this figure legend, the reader is referred to the web version of this article.)

observations are needed to see if the recent trend will continue, or whether the AMOC will recover to some degree.

While the proxy of AMOC from SLDIF indicates interesting variations in ocean dynamics, it cannot fully and equally represent all the components contributing to the AMOC observed by RAPID. For example, the low-frequency variations of AMOC (Fig. 7) are better represented by SLDIF than high-frequency variations, and wind-driven variations are represented by SLDIF at shorter lags relative to AMOC than density-

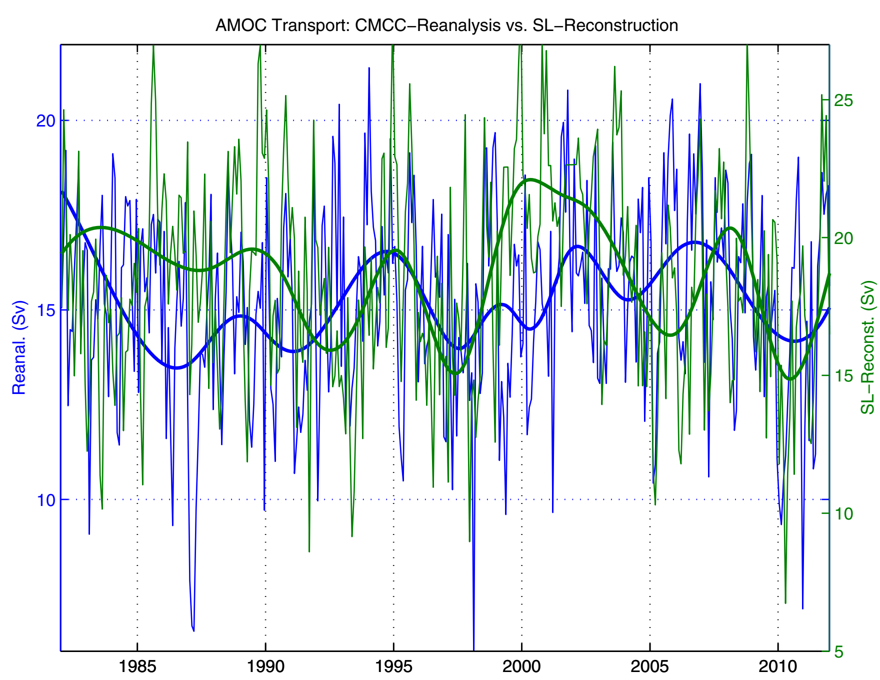

Fig. 10. Comparison of the AMOC transport reconstructed from sea level data (green; y-axis on the right) and the AMOC transport obtained from the reanalysis system of CMCC (blue; y-axis on the left). A 2-month lag was added (reanalysis leading the sea level proxy). Thin lines are monthly data and heavy smoother lines are the sum of the 3 lowest frequency EMD modes representing variations with periods of 5 yrs and longer. (For interpretation of the references to color in this figure legend, the reader is referred to the web version of this article.)

driven variations (Fig. 8). Since there is no observed “truth” of past AMOC variations, comparing our AMOC reconstruction with other estimates of AMOC can at least shed some light on common features. For example, there are some similarities between our results and the AMOC reconstruction based on SST shown in Klöwer et al. (2014), including the decline in 1960–1970 and after 2000. However, Klöwer et al.'s reconstruction represents mostly the low-frequency, heat-flux driven portion of AMOC at 48°N, while the RAPID data is for 26°N and includes high-frequency wind-driven variations. Another source of past AMOC estimates is from reanalysis systems that use a combination of numerical ocean models and data assimilation. Therefore, in Fig. 10 our AMOC reconstruction is compared with one such system, the CMCC Global Ocean Physical Reanalysis System (C-GLORS; Storto et al., 2011). Despite various uncertainties in the reanalysis estimates due to model biases, sparse data coverage and errors in the data assimilation calculations, the reanalysis and the reconstruction (with its own uncertainties as discussed before) are positively correlated at a statistically significant level ($C = 99\%$). The correlations between the two data sets are $R = 0.25$ for the raw monthly data (thin lines in Fig. 10), $R = 0.35$ for the low frequency modes (heavy lines in Fig. 10) and $R = 0.45$ for the seasonal cycle mode (not shown). High-frequency variations and a few anomalous points in the reanalysis seem to be reducing the overall correlation. The comparison reveals several interesting findings. First, the variability of the AMOC transport in the reanalysis is about 40% smaller than that of the reconstruction (note the different y-axis scales on the right and left of Fig. 10) and the mean AMOC transport in the reanalysis is ~3 Sv lower than in the reconstruction; both discrepancies are consistent with typical uncertainties in climate models (Roberts et al., 2014). Second, similar interannual variations with a ~5-year period are seen in both records. Third, in both records minima in AMOC transports are indicated around 1997 and 2010; other maxima and minima are seen in both records at around the same periods, but with additional ~1 year lag. The best correlation for 1935–2012 is obtained with the reconstruction record lagging by 2 months behind the reanalysis; this lag is similar to the lag found between the SLDIF and the RAPID data for 2004–2012, providing further support to the notion that the reconstruction correctly represents the underlying processes and the propagation of anomalies. This lag also confirms that variations in sea level are the result of changes in ocean currents, as proposed by Ezer et al. (2013) and others, and not the cause.

5. Summary and conclusions

The study addresses 3 issues. The first issue is the apparent disagreement between studies showing recent weakening in the GS (Ezer, 2013; Ezer et al., 2013) and in AMOC (Bryden et al., 2005; McCarthy et al., 2012; Srokosz et al., 2012; Smeed et al., 2013), while others suggest a stable GS over the past 20 yrs (Rossby et al., 2014). Comparisons between three independent data sets, the flow across a section from Bermuda to the U.S. coast obtained from the Oleander project, the AMOC transport obtained from the RAPID project and SLDIF obtained from tide gauges, reveal that all data sets are very consistent with each other and show similar variations, including the recent large downward trend in ocean currents in 2009–2010. There are two reasons for Rossby et al.'s contrasting results. First, the GS portion of the Oleander line used by Rossby et al. is largely influenced by eddies and recirculation gyres, so it was not correlated with the AMOC or even with the upstream GS (the FC transport). Only the flow through the entire Oleander line, that includes the Slope Current, the GS and the Sargasso Sea is correlated with AMOC. Second, because the AMOC trend is non-linear and affected by variations on many different scales (from weakly to multidecades), a mean slope calculated over a particular 20-year window may not mean much for the long-term trend (it's still short compared with the 60-year cycle, mentioned before), and does not represent most of the largest interannual changes, such as the weakening in 2009–2010. It was shown however, that when looking at the entire Oleander line, one sees the evidence of the large interannual variations, as seen in the other data sets. Another interesting result was that while the FC is not correlated with the Oleander GS downstream it is highly correlated with the GS position along the Oleander line, with a southward GS shift when FC transport increases, in agreement with previous studies (Joyce and Zhang, 2010). The position of the GS is also related to the Slope Current, in agreement with previous findings that show an increase in the Slope Current flow southward when the GS moved offshore (Ezer et al., 2013). The results suggest that the Slope Current is not the driver of the GS shift, but rather the result of it (additional impacts on the Slope Current from water sources in sub-polar regions are possible as well, but have not been discussed here).

The second goal of the study was to use the EMD/HHT analysis (Huang et al., 1998) to understand the relation between SLDIF and AMOC on different scales. The two time series are highly correlated with each other, and in particular, the drop in AMOC around 2010 seems to involve low frequency modes that can be detected in sea level. The EMD-derived trend over 2004–2012 is almost identical in AMOC and SLDIF and is clearly non-linear, pointing to difficulties in calculating linear trends from relatively short records. The wind-driven Ekman transport portion of AMOC is detected in the SLDIF record at all time scales, while the FC transport portion of AMOC is in phase with SLDIF for a 5 year cycle, but out of phase for the long-term trend. The mid-ocean portion of AMOC seems to lag behind SLDIF and the Ekman transport by ~2 yrs, indicating that variations in the mid-ocean flows may have been the result of climatic changes in wind patterns that have affected the density field and thus the geostrophic flow that contribute to the mid-ocean transport.

Finally, using the correlation between SLDIF and AMOC during 2004–2012, a reconstruction of 78 yrs of AMOC, 1935–2012, was obtained. This sea level-derived proxy for large-scale changes of flows may detect low-frequency and interannual variations in AMOC, in particular the wind-driven contributions, but is less accurate for detecting high-frequency variations. The reconstructed record indicates a long-term downward trend, as suggested by observations (Bryden et al., 2005) and predicted by climate models, but evaluating its significance requires further studies with other data. A comparison between the sea level-derived reconstruction of AMOC and reanalysis data for 1982–2012, shows surprisingly good agreement, despite obvious uncertainties in both estimates. Variations in the AMOC transport are dominated by interannual, decadal and multidecadal variations. The recent AMOC weakening that started around 2000 is comparable in its trend to the changes that occurred during the 1960s and 1970s, ~-4.5 Sv per decade. The potential consequences of the recent AMOC changes on slowing down the GS (Ezer et al., 2013) and accelerating sea level rise (Boon, 2012; Ezer and Corlett, 2012; Sallenger et al., 2012; Ezer, 2013), are quite similar to interpentadal changes reported between 1955–1959 and 1970–1974 (Greatbatch et al., 1991; Ezer et al., 1995). In both periods, the late 1960s to early 1970s and 2009–2010, NAO was significantly negative, which contributed to changes in the wind-driven Ekman transport and resulted in weakening GS. An important implication for coastal erosion and flooding of low-lying regions is the fact that during those periods sea level rose by ~10 cm over only few years, as observed in the past (Ezer et al., 1995) and in recent years (Sweet et al., 2009; Ezer and Atkinson, 2014; Goddard et al., 2015). The dramatic past changes (including a potential 30% weakening in the GS during the 1960s) were based on diagnostic numerical models that could not be completely verified, while the Oleander data, the altimeter data and the RAPID observations now provide valuable data to verify the recent changes. Continuing the monitoring of AMOC with the RAPID project will be very valuable for better understanding of climatic changes in ocean currents and evaluation of the long-term trend. Because of the lag found here between AMOC and sea level response, the RAPID monitoring may also have some predictive capabilities with implications for coastal sea level rise.

Acknowledgments

Old Dominion University's Climate Change and Sea Level Rise Initiative (CCSLRI) provided partial support for this study. R. Nicholls, I. D. Haigh and G. McCarthy are thanked for useful discussions and suggestions. Scientists at the National Oceanographic Centre (NOC), Southampton, UK, are thanked for providing the NEMO simulations (E. T. Blaker) and the RAPID data (available from: http://www.rapid.ac.uk/rapidmoc/). Members from T. Rossby's group at URI are thanked for providing the Oleander data, which are available from: http://www.po.gso.uri.edu/rafos/research/ole/. The tide gauges sea level data are available from the Permanent Service for Mean Sea Level (PSMSL) at: http://www.psmsl.org/. N. Pinardi and her group at CMCC, Italy, are thanked for helpful discussions and A. Storto is thanked for providing the reanalysis data, which are available at: http://c-glors.cmcc.bo.it/. Anonymous reviewers are thanked for useful suggestions that helped to improve the manuscript.

Appendix A. Acronyms and terms

ADCP — Acoustic Doppler Current Profiler; *AMO* — Atlantic Multidecadal Oscillations; *AMOC* — Atlantic Meridional Overturning Circulation; *AVISO* — Archiving, Validation and Interpretation of Satellite Oceanographic data; *CMCC* — The Euro-Mediterranean Center on Climate Change; *C-GLORS* — The CMCC Global Ocean Physical Reanalysis System; *EMD* — Empirical Mode Decomposition; *EEMD* — Ensemble Empirical Mode Decomposition; *FC* — Florida Current; *GIA* — Glacial Isostatic Adjustment; *GS* — Gulf Stream; *NAO* — North Atlantic Oscillation; *NEMO* — Nucleus for European Modelling of the Ocean; *PSMSL* — Permanent Service for Mean Sea Level; *RAPID* — (not an acronym) Observations to estimate AMOC transport; *SLDIF* — Sea Level Difference; *SLR* — Sea Level Rise; *SST* — Sea Surface Temperature.

A.1. Terms associated with the Oleander observations

OTF — Oleander Total Flux; *OGS* — Oleander Gulf Stream Flux; *OSC* — Oleander Slope Current Flux; *OSS* — Oleander Sargasso Sea Flux; *OPO* — Oleander Gulf Stream Position.

A.2. Terms associated with the RAPID observations

ATOT — AMOC Total Net Transport; *AFCT* — AMOC Florida Current transport; *AEKT* — AMOC Ekman transport; *AMOT* — AMOC Mid-ocean transport.

References

Atkinson, L.P., Ezer, T., Smith, E., 2013. Sea level rise and flooding risk in Virginia. Sea Grant Law Policy J. 5 (2), 3–14.

Baringer, M.O., McCarthy, G., Willis, J., Garzoli, S., Lankhorst, M., CMeinen, C.S., Send, U., Hobbs, W.R., Cunningham, S.A., Rayner, D., Smeed, D.A., Kanzow, T.O., Heimbach, P., Frajka-Williams, E., Macdonald, A., Dong, S., Marotzke, J., 2013. Meridional overturning circulation and heat transport observations in the Atlantic Ocean (in "State of the Climate in 2012"). Bull. Am. Meteorol. Soc. 94 (8), S65–S68.

Blaha, J.P., 1984. Fluctuations of monthly sea level as related to the intensity of the Gulf Stream from Key West to Norfolk. J. Geophys. Res. Oceans 89 (C5), 8033–8042.

Blaker, E.T., Hirschi, J.J.M., McCarthy, G., Sinha, B., Taws, S., Marsh, R., Coward, A., de Cuevas, B., 2014. Historical analogues of the recent extreme minima observed in the Atlantic meridional overturning circulation at 26°N. Clim. Dyn. http://dx.doi.org/10.1007/s00382-014-2274-6.

Boon, J.D., 2012. Evidence of sea level acceleration at U.S. and Canadian tide stations, Atlantic coast, North America. J. Coast. Res. 28 (6), 1437–1445. http://dx.doi.org/10.2112/JCOASTRES-D-12-00102.1.

Boon, J.D., Brubaker, J.M., Forrest, D.R., 2010. Chesapeake Bay land subsidence and sea level change. App. Mar. Sci. and Ocean Eng., Report No. 425. Virginia Institute of Marine Science, Gloucester Point, VA.

Bryden, H.L., Longworth, H.R., Cunningham, S.A., 2005. Slowing of the Atlantic meridional overturning circulation at 25°N. Nature 438. http://dx.doi.org/10.1038/nature04385.

Cazenave, A., Cozannet, G.L., 2014. Sea level rise and its coastal impacts. Earth's Future 2, 15–34. http://dx.doi.org/10.1002/2013EF000188.

Chambers, D.P., Merrifield, M.A., Nerem, R.S., 2012. Is there a 60-year oscillation in global mean sea level? Geophys. Res. Lett. 39, L18607. http://dx.doi.org/10.1029/2012GL052885.

Church, J.A., White, N.J., 2011. Sea-level rise from the late 19th to the early 21st century. Surv. Geophys. 32, 585–602. http://dx.doi.org/10.1007/s10712-011-9119-1.

Ezer, T., 1999. Decadal variabilities of the upper layers of the subtropical North Atlantic: an ocean model study. J. Phys. Oceanogr. 29 (12), 3111–3124. http://dx.doi.org/10.1175/1520-0485(1999)029.

Ezer, T., 2001. Can long-term variability in the Gulf Stream transport be inferred from sea level? Geophys. Res. Lett. 28 (6), 1031–1034. http://dx.doi.org/10.1029/2000GL011640.

Ezer, T., 2013. Sea level rise, spatially uneven and temporally unsteady: why the U.S. East Coast, the global tide gauge record, and the global altimeter data show different trends. Geophys. Res. Lett. 40, 5439–5444. http://dx.doi.org/10.1002/2013GL057952.

Ezer, T., Atkinson, L.P., 2014. Accelerated flooding along the U.S. East Coast: on the impact of sea-level rise, tides, storms, the Gulf Stream, and the North Atlantic Oscillations. Earth's Future 2 (8), 362–382. http://dx.doi.org/10.1002/2014EF000252.

Ezer, T., Corlett, W.B., 2012. Is sea level rise accelerating in the Chesapeake Bay? A demonstration of a novel new approach for analyzing sea level data. Geophys. Res. Lett. 39, L19605. http://dx.doi.org/10.1029/2012GL053435.

Ezer, T., Mellor, G.L., Greatbatch, R.J., 1995. On the interpentadal variability of the North Atlantic Ocean: model simulated changes in transport, meridional heat flux and coastal sea level between 1955–1959 and 1970–1974. J. Geophys. Res. 100 (C6), 10,559–10,566. http://dx.doi.org/10.1029/95JC00659.

Ezer, T., Atkinson, L.P., Corlett, W.B., Blanco, J.L., 2013. Gulf Stream's induced sea level rise and variability along the U.S. mid-Atlantic coast. J. Geophys. Res. 118, 685–697. http://dx.doi.org/10.1002/jgrc.20091.

Goddard, P.B., Yin, J., Griffies, S.M., Zhang, S., 2015. An extreme event of sea-level rise along the Northeast coast of North America in 2009–2010. Nat. Commun. http://dx.doi.org/10.1038/ncomms7346.

Greatbatch, R.J., Fanning, A.F., Goulding, A.D., Levitus, S., 1991. A diagnosis of interpentadal circulation changes in the North Atlantic. J. Geophys. Res. 96 (C12), 22009–22023. http://dx.doi.org/10.1029/91JC02423.

Griffies, S.M., Yin, J., Durack, P.J., Goddard, P., Bates, S.C., Behrens, E., Bentsen, M., Daohua, B., Biastoch, A., Böning, C.W., Bozec, A., Chassignet, E., Danabasoglu, G., Danilov, S., Domingues, C.M., Drange, H., Farneti, R., Fernandez, E., Greatbatch, R.J., Holland, D.M., Ilicak, M., Large, W.G., Lorbacher, K., Lu, J., Marsland, S.J., Mishra, A., Nurser, G., Salas, D., Mélia, Y., Palter, J.B., Samuels, B.L., Schröter, J., Schwarzkopf, F.U., Sidorenko, D., Treguier, A.M., Tseng, Y., Tsujino, H., Uotila, P., Valcke, S., Voldoire, A., Wang, Q., Winton, M., Zhang, X., 2014. An assessment of global and regional sea level for years 1993–2007 in a suite of interannual CORE-II simulations. Ocean Model. 78, 35–89. http://dx.doi.org/10.1016/j.ocemod.2014.03.004.

Haigh, I.D., Wahl, T., Rohling, E.J., Price, R.M., Battiaratchi, C.B., Calafat, F.M., Dangendorf, S., 2014. Timescales for detecting a significant acceleration in sea level rise. Nat. Commun. http://dx.doi.org/10.1038/ncomms4635.

Hakkinen, S., Rhines, P.B., 2004. Decline of subpolar North Atlantic circulation during the 1990s. Science 304, 555–559. http://dx.doi.org/10.1126/science.1094917.

Huang, N.E., Shen, Z., Long, S.R., Wu, M.C., Shih, E.H., Zheng, Q., Tung, C.C., Liu, H.H., 1998. The empirical mode decomposition and the Hilbert spectrum for non-stationary time series analysis. Proc. R. Soc. London, Ser. A 454, 903–995.

Huang, N.E., Wu, M.C., Long, S.R., Shen, S.S., Qu, W., Gloersen, P., Fan, K.L., 2003. A confidence limit for the empirical mode decomposition and Hilbert spectral analysis. Proc. R. Soc. London, Ser. A 459 (2037), 2317–2345. http://dx.doi.org/10.1098/rspa.2003.1123.

Joyce, T.M., Zhang, R., 2010. On the path of the Gulf Stream and the Atlantic meridional overturning circulation. J. Clim. 23, 3146–3154. http://dx.doi.org/10.1175/2010JCLI3310.1.

Joyce, T.M., Deser, C., Spall, M.A., 2000. The relation between decadal variability of subtropical mode water and the North Atlantic oscillation. J. Clim. 13, 2550–2569. http://dx.doi.org/10.1175/1520-0442(2000)013.

Kenigson, J.S., Han, W., 2014. Detecting and understanding the accelerated sea level rise along the east coast of US during recent decades. J. Geophys. Res. http://dx.doi.org/10.1002/2014JC010305.

Klöwer, M., Latif, M., Ding, H., Greatbatch, R.J., Park, W., 2014. Atlantic meridional overturning circulation and the prediction of North Atlantic sea surface temperature. Earth Planet. Sci. Lett. 406 (15), 1–6. http://dx.doi.org/10.1016/j.epsl.2014.09.001.

Kopp, R.E., 2013. Does the mid-Atlantic United States sea-level acceleration hot spot reflect ocean dynamic variability? Geophys. Res. Lett. 40 (15), 3981–3985. http://dx.doi.org/10.1002/grl.50781.

Levermann, A., Griesel, A., Hofmann, M., Montoya, M., Rahmstorf, S., 2005. Dynamic sea level changes following changes in the thermohaline circulation. Clim. Dyn. 24 (4), 347–354.

Levitus, S., 1989. Interpentadal variability of temperature and salinity at intermediate depths of the North Atlantic Ocean, 1970–1974 versus 1955–1959. J. Geophys. Res. 94, 6091–6131.

Levitus, S., 1990. Interpentadal variability of steric sea level and geopotential thickness of the north Atlantic Ocean, 1970–1974 versus 1955–1959. J. Geophys. Res. 95 (C4), 5233–5238. http://dx.doi.org/10.1029/JC095iC04p05233.

Lorbacher, K., Dengg, J., Böning, C.W., Biastoch, A., 2010. Regional patterns of sea level change related to interannual variability and multidecadal trends in the Atlantic meridional overturning circulation. J. Clim. 23 (15), 4243–4254. http://dx.doi.org/10.1175/2010JCLI3341.1.

McCarthy, G., Frejka-Williams, E., Johns, W.E., Baringer, M.O., Meinen, C.S., Bryden, H.L., Rayner, D., Duchez, A., Roberts, C., Cunningham, S.A., 2012. Observed interannual variability of the Atlantic meridional overturning circulation at 26.5°N. Geophys. Res. Lett. http://dx.doi.org/10.1029/2012GL052933.

Miller, K.G., Kopp, R.E., Horton, B.P., Browning, J.V., Kemp, A.C., 2013. A geological perspective on sea-level rise and its impacts along the U.S. mid-Atlantic coast. Earth's Future 1, 3–18. http://dx.doi.org/10.1002/2013EF000135.
Nicholls, R.J., Cazenave, A., 2010. Sea-level rise and its impact on coastal zones. Science 328 (5985), 1517–1520. http://dx.doi.org/10.1126/science.1185782.
Roberts, C.D., Jackson, L., McNeall, D., 2014. Is the 2004–2012 reduction of the Atlantic meridional overturning circulation significant? Geophys. Res. Lett. 41. http://dx.doi.org/10.1002/2014GL059473.
Rossby, T., Flagg, C., Donohue, K., 2010. On the variability of Gulf Stream transport from seasonal to decadal timescales. J. Mar. Res. 68, 503–522.
Rossby, T., Flagg, C.N., Donohue, K., Sanchez-Franks, A., Lillibridge, J., 2014. On the long-term stability of Gulf Stream transport based on 20 years of direct measurements. Geophys. Res. Lett. 41, 114–120. http://dx.doi.org/10.1002/2013GL058636.
Sallenger, A.H., Doran, K.S., Howd, P., 2012. Hotspot of accelerated sea-level rise on the Atlantic coast of North America. Nat. Clim. Change 2, 884–888. http://dx.doi.org/10.1038/NCILMATE1597.
Smeed, D.A., McCarthy, G., Cunningham, S.A., Frajka-Williams, E., Rayner, D., Johns, W.E., Meinen, C.S., Baringer, M.O., Moat, B.I., Duchez, A., Bryden, H.L., 2013. Observed decline of the Atlantic Meridional Overturning Circulation 2004 to 2012. Ocean Sci. Discuss. 10, 1619–1645. http://dx.doi.org/10.5194/osd-10-1619-2013.
Srokosz, M., Baringer, M., Bryden, H., Cunningham, S., Delworth, T., Lozier, S., Marotzke, J., Sutton, R., 2012. Past, present, and future changes in the Atlantic meridional overturning circulation. Bull. Am. Meteorol. Soc. 1663–1676 http://dx.doi.org/10.1175/BAMS-D-11-00151.1.
Storto, A., Dobricic, S., Masina, S., Di Pietro, P., 2011. Assimilating along-track altimetric observations through local hydrostatic adjustment in a global ocean variational assimilation system. Mon. Weather Rev. 139, 738–754.
Sturges, W.B., Hong, G., 1995. Wind forcing of the Atlantic thermocline along 32°N at low frequencies. J. Phys. Oceanogr. 25, 1706–1715.
Sturges, W.B., Hong, G., 2001. Gulf Stream transport variability at periods of decades. J. Phys. Oceanogr. 31, 1304–1312.
Sweet, W., Zervas, C., Gill, S., 2009. Elevated East Coast Sea Level Anomaly: June–July 2009, NOAA Tech. Rep. No. NOS CO-OPS 051. NOAA Natl. Ocean Service, Silver Spring, Md (40 pp.).
Thompson, P.R., Mitchum, G.T., 2014. Coherent sea level variability on the North Atlantic western boundary. J. Geophys. Res. Oceans 119, 5676–5689. http://dx.doi.org/10.1002/2014JC009999.
Woodworth, P.L., Player, R., 2003. The permanent service for mean sea level: an update to the 21st century. J. Coast. Res. 19 (2), 287–295.
Woodworth, P.L., Maqueda, M., Roussenov, M.Á., Williams, V.M., Hughes, R.G., 2014. Mean sea level variability along the northeast American Atlantic coast, and the roles of the wind and the overturning circulation. J. Geophys. Res. Oceans http://dx.doi.org/10.1002/2014JC010520.
Wu, Z., Huang, N.E., 2009. Ensemble empirical mode decomposition: a noise-assisted data analysis method. Adv. Adapt. Data Anal. 1 (01), 1–41.
Wu, Z., Huang, N.E., Long, S.R., Peng, C.-K., 2007. On the trend, detrending and variability of nonlinear and non-stationary time series. Proc. Natl. Acad. Sci. U. S. A. 104, 14889–14894.
Yin, J., Goddard, P.B., 2013. Oceanic control of sea level rise patterns along the East Coast of the United States. Geophys. Res. Lett. 40, 5514–5520. http://dx.doi.org/10.1002/2013GL057992.
Yin, J., Schlesinger, M.E., Stouffer, R.J., 2009. Model projections of rapid sea-level rise on the northeast coast of the United States. Nat. Geosci. 2, 262–266. http://dx.doi.org/10.1038/NGEO462.
Zhao, J., Johns, W., 2014. Wind-forced interannual variability of the Atlantic Meridional Overturning Circulation at 26.5°N. J. Geophys. Res. Oceans 119, 6253–6273. http://dx.doi.org/10.1002/2013JC009407.